Journal of Glaciology

Article

Cite this article: Svendsen SP, Gjermundsen EF, Sund M, Anjar J (2025) Slushflows: Large discrepancy between reported and actual incidents. *Journal of Glaciology* **71**, e96, 1–12. https://doi.org/10.1017/jog.2025.10069

Received: 15 November 2024
Revised: 20 June 2025
Accepted: 25 June 2025

Keywords
Slushflows; gravity flows; snow; remote sensing; hazard management

Corresponding author:
Sunniva Pauline Svendsen;
Email: sunniva.p.svendsen@usn.no

cambridge.org/jog

Slushflows: Large discrepancy between reported and actual incidents

Sunniva Pauline Svendsen[1], Endre Før Gjermundsen[2], Monica Sund[3] and Johanna Anjar[2]

[1]Natural Sciences and Environmental Health, University of South-Eastern Norway, Bø i Telemark, Norway; [2]Department of Business and IT, University of South-Eastern Norway - Campus Bø, Bø i Telemark, Norway and [3]Hydrology Department, The Norwegian Water Resources and Energy Directorate, Oslo, Norway

Abstract

A key challenge in advancing slushflow management is the limited record of past incidents. Identifying their starting points and enhancing the quality of slushflow documentation are important in order to improve the regional early warning and develop slushflow numerical runout models and susceptibility maps. Here we investigate three major slushflow events at Kistrandfjellet, northern Norway and quantify the differences between registered slushflows in the national rapid mass movement database and the actual events. We use unique image datasets from the events in February 2021, January 2023 and January 2024, and identify slushflow starting points and flow paths. The curvature of the starting point locations is examined to assess how local topography influences slushflow release at the field site. Our mapping reveals 25 slushflows across the three events, whereas only five were registered in the database. For the 2021 event, we found six times as many slushflows as were officially registered. Comparison of our mapped slushflows to modeled drainage pathways and FKB-Vann (the official surface water dataset of Norway), yielded an average overlap of 35%. To improve slushflow management, we recommend establishing a standardized protocol for future data collection.

1. Introduction

Slushflows are a distinct type of mass movement characterized by a rapid downslope flow of water-saturated snow, often containing soil, rock debris and vegetation (Washburn and Goldthwait, 1958; Rapp, 1960; Hestnes, 1985, 1998; Nyberg, 1985; Hestnes and others, 1994). Slushflows frequently initiate along drainage pathways during periods of rainfall and/or snowmelt (Rapp, 1960; Hestnes, 1985, 1998; Nyberg, 1985; Hestnes and others, 1994). These drainage pathways often originate in depressions or topographic steps where water may accumulate in the snow. The buildup of water within the snowpack is a prerequisite for slushflow initiation and is typically associated with relatively gentle topography (0–30°) in the release area (Luckman, 1977; Hestnes, 1985, 2010; Nyberg, 1985; Onesti, 1985). This contrasts with the steeper terrain conducive to the release of snow avalanches and debris flows. Nevertheless, slushflows are not confined to low-relief areas but may occur in various topographic settings. For example, they may initiate on shallow gradients within otherwise steep, high-relief mountain slopes, as well as on low-relief terrain, such as open lowlands typically marked by bogs or lakes (Hestnes, 1985, 1998; Hestnes and others, 1994). Due to their high water content, slushflows behave as a viscous fluid when moving downslope and typically will not decelerate until they encounter nearly flat terrain (Hestnes, 1985; Perov, 1998). In areas with sufficient debris cover, slushflows erodes the ground surface through direct scouring and ploughing, resulting in the downslope transport and subsequent deposition of snow and sediments (Clark and Seppala, 1988; Nyberg, 1989; Decaulne and Sæmundsson, 2006). Because of their high density, speed and erosional power, slushflows are capable of generating particularly destructive impacts and pose significant hazards to both human life and infrastructure in Norway (Hestnes, 1985, 1998; Hestnes and Sandersen, 2000; Hestnes and Bakkehøi, 2004).

A regional early warning for slushflow hazards was established during 2013-14 by the Norwegian Water Resources and Energy Directorate (NVE) (Sund and others, 2024). The regional slushflow early warning assessment method involves three main variables important to the triggering process: ground conditions, snow properties, and rainfall and/or snowmelt. These data are obtained from gridded forecasting model simulations, real-time data from automatic weather stations and field observations. The assessment of the different variables is currently performed manually by the forecasters.

A key challenge in advancing the early warning assessment method is the limited record of past slushflow incidents due to both underreporting and misidentifications, where slushflows were incorrectly categorized as other types of rapid mass movements, such as snow avalanches

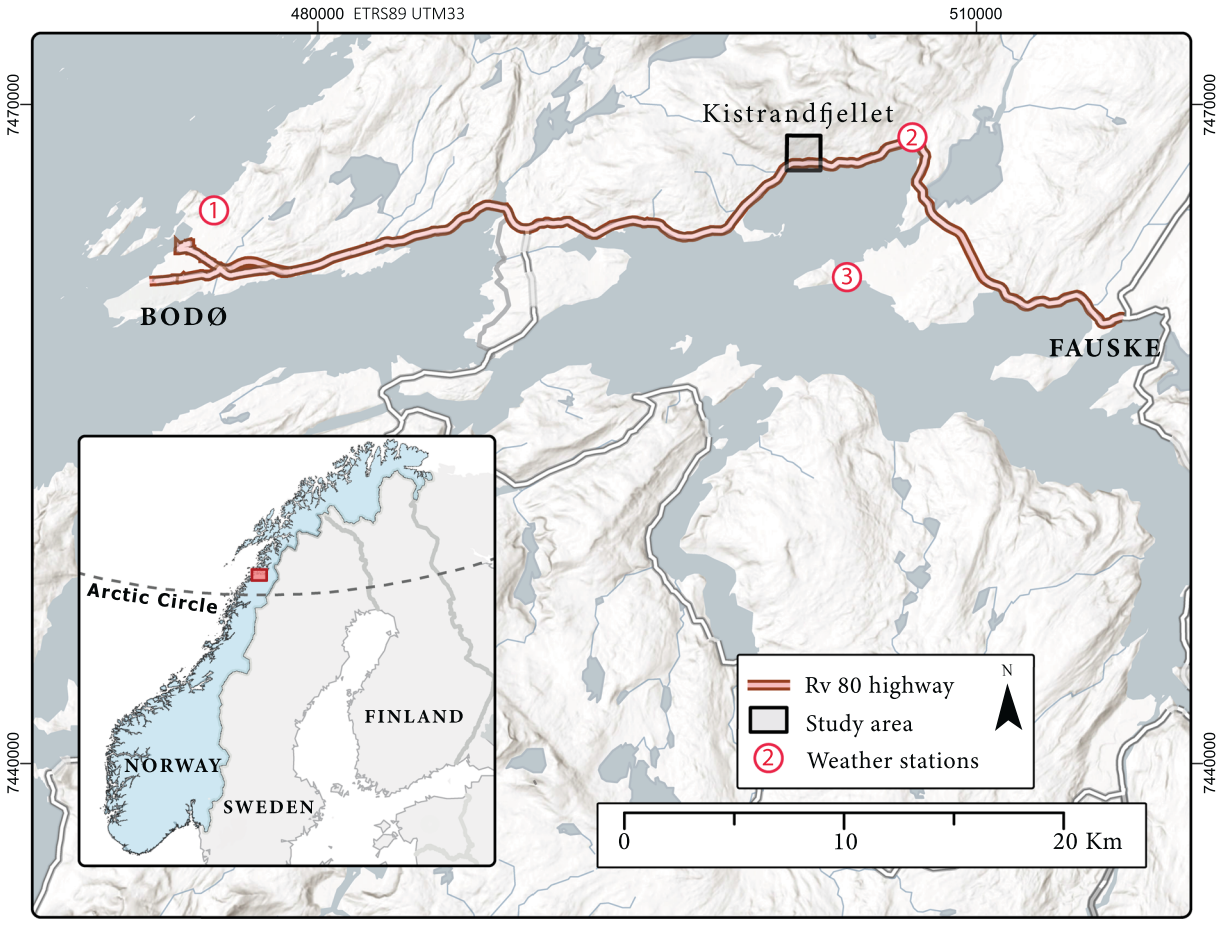

Figure 1. Overview of the Rv-80 highway, along with locations of the field site and weather stations.

and debris flows (Hestnes and Sandersen, 1987; Onesti and Hestnes, 1989; Hestnes and others, 2012; Hestnes and Jaedicke, 2018; Jaedicke and others, 2024; Sund and others, 2024). The relatively low preservation potential of slushflow deposits makes identification from remote sensing challenging (Sund and others, 2024; Svendsen and others, 2024) compared to other gravity flows, such as landslides and debris flows, which typically leaves longer-lasting tracks on the ground. In addition, existing records exhibit a spatial bias towards roads and infrastructure, with registered slushflow incidents typically containing the most information at the locations where they intersect with infrastructure. In contrast, data on starting points are often either incomplete or missing. This is unfortunate, as knowledge of the starting points is needed to link slushflow to hydrological and meteorological data at the time of slushflow release. Such data are important for the establishment of an index tool for the regional slushflow early warning (Sund and others, 2024), to develop numerical runout models, and as input to future slushflow susceptibility maps.

Slushflow-related road closures occur annually in Norway. A well-known problem area lies east of Bodø in northern Norway (Fig. 1), where slushflows frequently disrupts traffic along the main roadway into the city. On 25 February 2021, a slushflow event resulted in a fatality, while two events on 25 January 2023 and 9 January 2024 led to extended road closures (Andreassen, 2023; Andreassen and others, 2024). Such closures have caused economic losses in the order of 5 million NOK per day (Avisa Nordland, 2024), demonstrating the urgent need for the protective dams currently under construction.

To improve slushflow management, we examine the consistency between reported slushflow incidents and actual occurrences from three slushflow events, based on the unique aerial imagery available at this site. We identify slushflow starting points and flow paths for each of the three events to assess whether the slushflow incidents reported to the database reflect the true scope of slushflow activity. There are three main objectives: (i) To identify and map slushflow starting zones and flow paths from the available imagery; (ii) To compare the findings from the three slushflow events with observations reported to the national rapid mass movement database; and (iii) To investigate the relationship between mapped slushflow paths, modeled drainage pathways, and the official surface water dataset of Norway ('FKB-Vann').

2. Field site and data

2.1. Field site

Kistrandfjellet mountain (with peaks up to 982 m a.s.l.) is situated ~25 km east of Bodø, the largest city in Nordland County, Northern Norway (Fig. 1). The area experiences a maritime climate with a mean annual air temperature of 4.1°C and mean annual precipitation of 1070 mm (values for Fauske, see Fig. 1) (Norwegian Centre for Climate Services, 2022). A coastal east-west

https://doi.org/10.1017/jog.2025.10069 Published online by Cambridge University Press

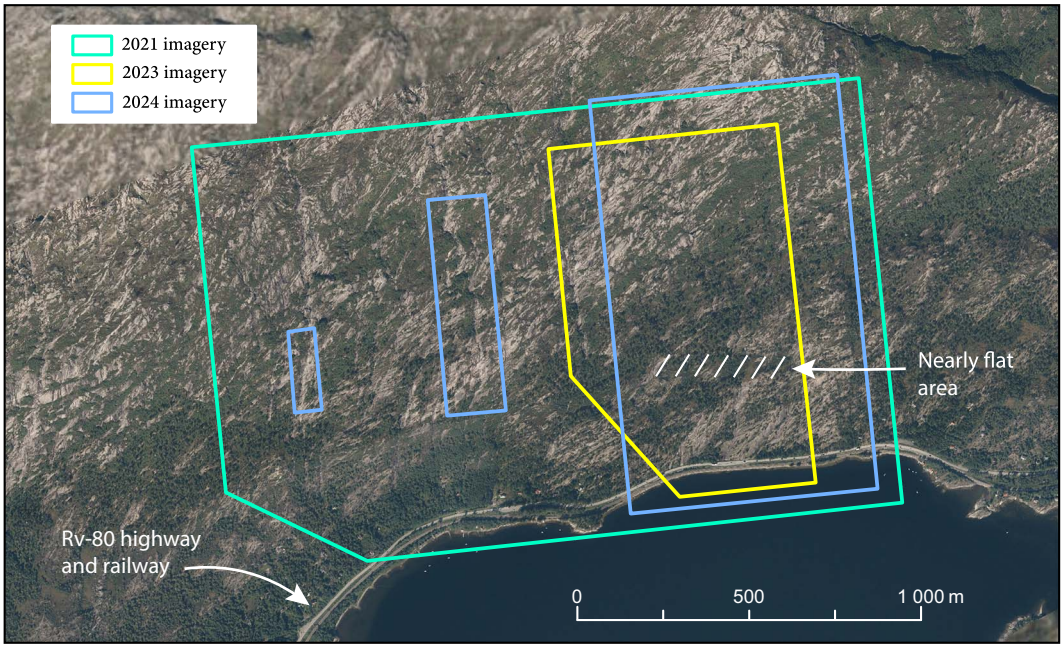

Figure 2. Area coverage of the image datasets for the three events.

transportation route links Bodø to the surrounding urban areas. The route comprises both the Nordland railway line and the Rv-80, a 59.8 km two-lane highway that is among the busiest in northern Norway (Andreassen, 2023). Mountain slopes along the Rv-80 have southernly aspects and rise up to 1050 m a.s.l. The Rv-80 and the adjacent railway traverse the base of Kistrandfjellet at near sea level. The mountainside is characterized by exposed rock surfaces and bedrock slabs, with minimal sediment cover. Vegetation is sparse, primarily consisting of shrubs and light pine forest at lower elevations. At ~85 m a.s.l., the gradient decreases to form a nearly flat area (see Fig. 2). Numerous small streams drain the south-facing slopes and pass beneath the Rv-80 and railway via culverts before emptying into the fjord.

Table 1. Overview of the image datasets used in this study

Year	Acquisition method	Date of capture	Source
2021 image dataset	Panasonic DMC-FZ200 camera (from helicopter)	25 Feb 2021, i.e. on the day of the event	330 Squadron, Royal Norwegian Air Force
2023 image dataset	DJI Matrice 300 RTK drone	26 Jan 2023, i.e. 1 day after the event	Norwegian Public Roads Administration (NPRA)
2024 image dataset	DJI Matrice 300 RTK drone	9–10 Jan 2024, i.e. on the day of the event and the following day	NPRA

2.2. Slushflow imagery and historical records

The image datasets used in this study comprise photographs captured from a helicopter (2021) and images recorded with an Unmanned Aerial Vehicle (UAV) (2023 and 2024) (Table 1), each with varying coverage (Fig. 2). The 2021 dataset consists of oblique images recorded with a handheld camera, providing detailed coverage across a large area, including high-elevation views (Fig. 3). The 2023 and 2024 UAV image datasets include both oblique and vertical viewing angles (Fig. 3). While the 2021 dataset was captured opportunistically, both the 2023 and 2024 datasets were specifically captured to evaluate the ongoing slushflow risk to the Rv-80. The onset of frequent slushflows impacting a heavily trafficked highway at this location in 2021 (Andreassen, 2023) led to greater documentation than what is currently available at other sites. Integration and utilization of various image types such as handheld cameras during commercial flights have been demonstrated by Eiken and Sund (2012).

In Norway, slushflow observations are registered through Varsom Regobs, a crowdsourcing tool used for recording natural hazards in real-time (Ekker and others, 2013; Sund and others, 2024). These observations are transferred to a national rapid mass movement database, accessible at www.skredregistrering.no, where they subsequently undergo quality assessment (Lunde and others, 2023; Sund and others, 2024). Important parameters of varying accuracy are stored in the slushflow section of the database, including the timing of occurrence, runout zone locations and snow deposit volumes. Records in the database show a clustering along the Rv-80, particularly where it traverses Kistrandfjellet. For our analysis, we selected all slushflows registered in the study area from the three selected events. Because a few incidents had multiple entries in the 2021 and 2023 events, all registrations were carefully assessed to avoid duplications.

2.3. Meteorological data

Air temperature and precipitation data for the 4 days leading up to and including each event day are presented in Table 2. The data were obtained from three weather stations along the RV-80, see Figure 1 (Norwegian Centre for Climate Services, 2025). Air temperature data were sourced from the two closest stations (No. 2, situated ~4.3 km east of the field site at 5 m a.s.l.) and station No. 3 (situated ~5.3 km south at 20 m a.s.l.). As precipitation

https://doi.org/10.1017/jog.2025.10069 Published online by Cambridge University Press

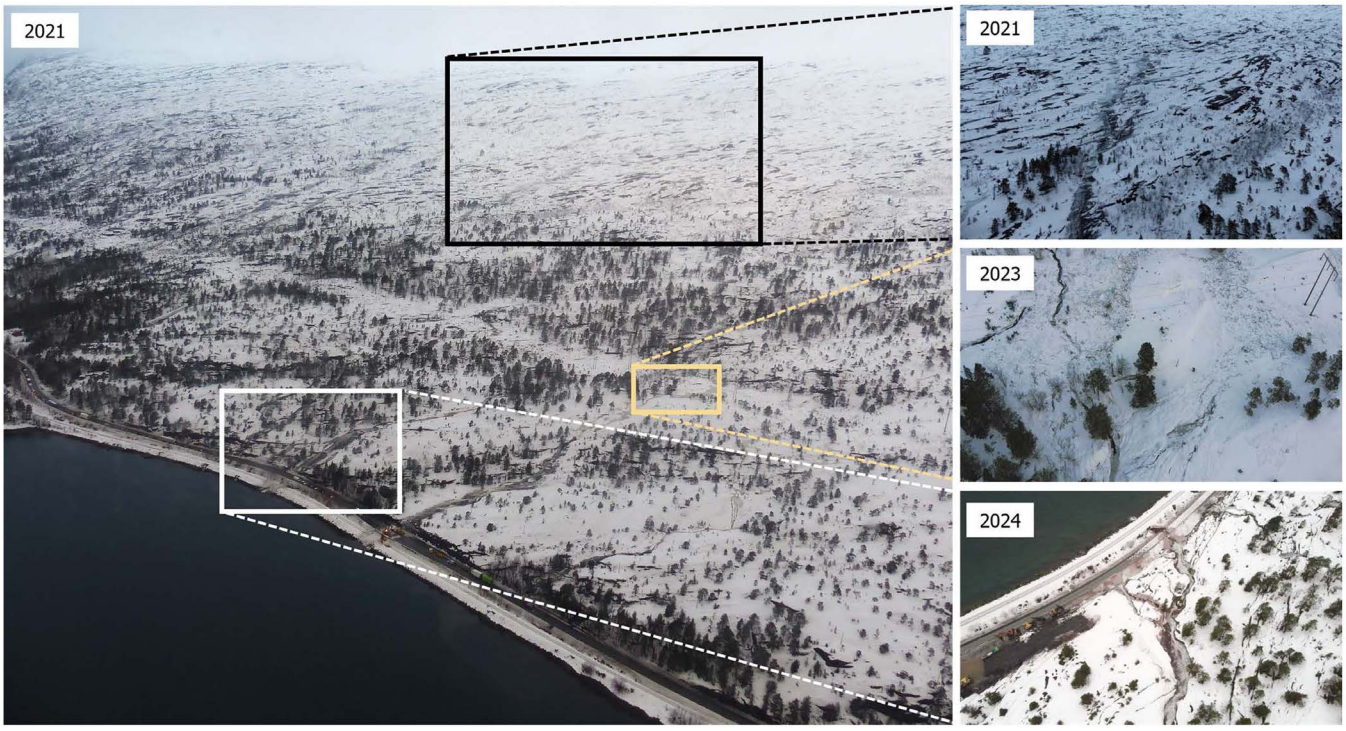

Figure 3. Examples of photographs from all three image datasets. The 2021 dataset provided the most extensive coverage, with some images capturing nearly the entire field site.

Table 2. Mean daily air temperature and total daily precipitation values for the days preceding and including the day of each event

		Precipitation (mm)	Mean daily temperature (°C)	Snow observations in Varsom Regobs	Simulated snow depth at starting locations (cm)	
2021 event	Weather stations	WS 1	WS 2			
	21 Feb	0,9	−5.9	Depth hoar registered ∼14 km east of the field site on 24 Feb 2021	No. 4	51.1
	22 Feb	11.5	−4.1		No. 6II	44.2
	23 Feb	0	−3.5		No. 9	27.8
	24 Feb	0.5	2.5		No. 10	27.8
	25 Feb	**23.7**	**3.8**		No. 11	27.8
					Avg.	**35.7**
2023 event	Weather stations	WS 3	WS 3			
	21 Jan	7.2	1.6	Depth hoar registered ∼2.5 km northeast of the field site on 19 Jan 2023	No. 4	106.1
	22 Jan	3.7	5.2		No. 6II	68.0
	23 Jan	1.8	3.9		No. 9	16.5
	24 Jan	9.4	2.3		No. 10	16.5
	25 Jan	**42.4**	**3.5**		No. 11	16.5
					Avg.	**44.7**
2024 event	Weather stations	WS 3	WS 2			
	05 Jan	0.1	−6	Facets registered near the bottom of a snowpack ∼6 km east of the field site on 7 Jan 2024	No. 4	89.5
	06 Jan	5.5	−3.9		No. 6II	86.6
	07 Jan	0.2	−0.7		No. 9	36.7
	08 Jan	7.5	3.6		No. 10	36.7
	09 Jan	**40.8**	**5.6**		No. 11	36.7
					Avg.	**57.2**

Slushflow event days are indicated in bold. Snow observations prior to the events, as well as simulated snow depth at starting locations from senorge.no at 06.00 UTC on the event days, are shown in the rightmost columns.

data were incomplete from these two stations, data for the 2021 event were obtained from station No. 1 in Bodø (situated ∼25.7 km west at 5 m a.s.l.). It is worth noting that all stations are situated near sea level, whereas slushflow starting points will be located at higher elevations, where conditions may differ. For the 2021 and 2024 events, temperatures increased from just below freezing to above freezing, constituting rises of 9.7°C and 11.6°C in the span of 5 days, respectively. For the 2023 event, the temperature fluctuated above freezing and rose slightly further toward the event, constituting a 1.9°C increase over the 5-day period. Further, rainfall (23.7–42.4 mm) is recorded on each event day. Some caution should be applied to the precipitation levels for the 2021 event given the difference in values recorded at weather station No. 1, located in the relatively open terrain of Bodø, and station No. 2, situated further inland along the fjord and surrounded by high mountains. For all events, little to no precipitation fell on the preceding days, whereas on each event day, precipitation in the order of 23.7–42.4 mm was recorded.

https://doi.org/10.1017/jog.2025.10069 Published online by Cambridge University Press

Occasional observations of snow profiles and stratigraphy are registered in Varsom Regobs. Three entries made 1–6 days prior to all event days indicate the presence of either depth hoar or facets in snowpacks in and around the study area (https://www.regobs.no/registration/257613 (NVE, 2021), https://www.regobs.no/registration/322704 (NVE, 2023), https://www.regobs.no/registration/362433 (NVE, 2024).

Simulated snow depth values at slushflow starting locations from www.senorge.no (previously www.Xgeo.no) at 06.00 UTC on the event days are given in Table 2 (SeNorge, 2025). Values are simulated in a 1 km × 1 km grid. Average snow depth values of the *SeNorge* grid cells that surround five starting locations in which slushflows were triggered in more than one event (Nos. 4, 6II, and 9–11) are given below the specific grid values. The *SeNorge* snow depths are interpolated from precipitation and temperature data recorded at monitoring stations within the observation network of the Norwegian Meteorological Institute. As such, the snow depth values should be treated only as rough estimates. Errors in the *SeNorge* snow maps could be a result of errors and uncertainties in the precipitation and temperature interpolation or that the model simulates conditions differently than they are. Particularly when the air temperature is ∼0°C, errors and uncertainty in the interpolation and the snow depth calculation can lead to large errors in the snow depth values. The coarse resolution of the snow model also inhibits representation of local variability in snow accumulation due to wind transportation and small-scale topography. At Kistrandfjellet, where the topography is undulating and the vegetation sparse, differences in snow accumulation may be substantial. For example, during field work on 27 January 2023, 2 days following the 2023 event, the snow depth in the central, lower part of the field site was measured to ∼50 cm, while the corresponding simulated depth from *SeNorge* was 16.5 cm.

3. Methods

3.1. Mapping of slushflow activity

Mapping of slushflow starting positions, flow paths and runout zones was conducted to examine the three slushflow events at Kistrandfjellet. While no unified protocol for identifying slushflows currently exists, they can be recognized based on several characteristics, such as their dark-colored, water-saturated snow, continuous flow paths and snow transport. The flow path of a slushflow will form a continuous feature as it flows downslope due to the saturated state of the snow. Identifying these flow paths may be particularly difficult in areas with ice patches or snowpacks with surface water drainage. To differentiate between ice patches and slushflows, potential flow paths that are interrupted by undisturbed snow surfaces are interpreted as frozen streams. Conversely, continuous flow paths are identified as slushflows, indicating the transportation of water and snow along their entire course. Snowpacks with surface water drainage may also resemble a slushflow path. Such drainage paths lack snow transport, however, which identifies them as open streams rather than slushflows. For slushflows, the ground is the gliding surface in central parts of the flow path (Hestnes, 1998), necessitating the transport of snow.

Particular emphasis was placed on identifying slushflow starting locations. These may vary in size and morphology based on terrain characteristics, ranging from small and linear in shape for slushflows that release along drainage pathways to larger and more distinctive features for those that release on open slopes, bogs and depressions (Hestnes, 1985). The starting location, at the uppermost point of the flow path, is interpreted as the point where the snow surface transitions into a darker-colored area, often with water draining over the bedrock topography. As this is where the mass movement of water-saturated snow begins, the starting zone will contrast with the white, undisturbed snow above. In our analysis, starting zones were mapped at the highest visible points of flow paths and, due to their generally narrow, channelized form at our field site, were marked with a single point feature (Fig. 4).

Starting zones, flow paths and runout zones were drawn in ArcGIS Pro 3.2.1 using orthophotos (Norgeibilder, 2022) and Digital Elevation Models (DEMs) downloaded from www.hoydedata.no (Hoydedata, 2017), provided by the Norwegian Mapping Authority (Project: NDH Bodø 2pkt 2017, spatial resolution: 0.5 m). Mapping of the 2023 event was supplemented by field observations conducted 2 days after the event, when the Rv-80 reopened on 27 January 2023. Fieldwork was also carried out in June 2024 to search for potential sediment traces of slushflow activity.

3.2. Modeling of drainage pathways

Slushflows often flow along streams and drainage pathways on mountain slopes. To investigate the potential relationship between slushflows and surface water drainage in the study area, we modeled the flow accumulation of surface water on the south-facing slopes of Kistrandfjellet. The drainage pathways were generated with the Flow Accumulation tool in ArcGIS Pro 3.2.1 using a DEM with a 0.5 m resolution. The Flow Accumulation geoprocessing tool models the accumulated waterflow to each cell of the DEM, based on the flow direction of water across a surface. Water will flow from one cell to the neighboring cell with lowest elevation, and the flow accumulation tool calculates the number of upstream cells that flow into the cells in the output raster. By defining the size of area (the number of cells) needed to create a stream, we can generate a stream network. The stream network represents areas of concentrated flow. We used an upstream area of 5 acres (5000 m^2), implying that only cells receiving flow from more than 20 000 upstream cells (5000 m^2) would end up as a 'stream' in the resulting raster. The resulting flow accumulation raster was finally converted to vector. Due to limited debris cover and sparse vegetation on the mountain, water infiltration into soil was considered negligible and thus not included in the model. The effect of snow cover was not included due to the coarse resolution of available snow depth data (see Section 2.3).

The modeled stream pathways were compared to the mapped slushflows both visually and statistically. For the statistical approach, overlay analysis between our mapped slushflows and the modeled streams was performed, assuming an average width of 3 m for the mapped slushflows and modeled streams with no width.

Further, the mapped slushflows were compared to the official surface water dataset in Norway, *FKB-Vann (Geonorge, 2024)*. FKB is a collection of official datasets in Norway and comes from a collaboration between public and private partners (available from https://www.geonorge.no/). The FKB include datasets on, e.g. area use, buildings, roads and water, and are typically updated around every fifth year. FKB-Vann includes lakes, streams and rivers and is produced photogrammetrically, i.e. digitized manually on orthophotos with a spatial resolution as fine as 0.1 m (Geonorge). Orthophotos is normally recorded during the summer months,

https://doi.org/10.1017/jog.2025.10069 Published online by Cambridge University Press

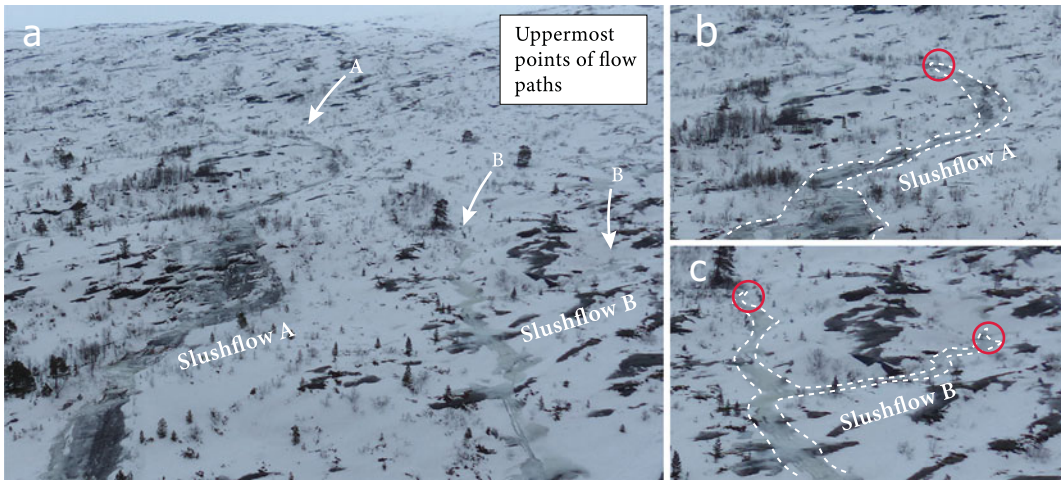

Figure 4. Example of interpreted starting points from the 2021 event imagery. (a) Sslushflow paths forming gray-colored, continuous features on the mountain slope, surrounded by white snow and exposed bedrock. Their uppermost points are identified. (b and c) Close-up view of the upper parts of slushflow A and B from image (a). Starting locations are marked with a single point. Slushflow A initiated from a single starting zone, whereas slushflow B initiated from two separate starting zones.

and the timing of image acquisition will influence the number of visible streams. Hence, an exact overlap between the modeled streams and FKB-Vann is not expected. The same overlay procedure was run between our mapped slushflows and FKB-Vann.

4. Results

4.1. The 2021 event

Analysis of the 2021 image dataset revealed 12 slushflows descending from elevations of up to ∼300 m a.s.l. (Table 3, Fig. 5). The longest slushflow path (No. 6) covered a distance of ∼900 m. Two slushflows, Nos. 2 and 4, separate into multiple paths as they flow downslope (indicated by letters, e.g. No. 2a-b), while three slushflows, Nos. 5, 6 and 8, initiate from separate starting zones and converge downslope (indicated by Roman numerals, e.g. No. 5I-II) (see Table 3, Fig. 5). The starting locations vary in terms of both topography and substrate. The majority are situated near streams on sloping rock surfaces with sparse or no vegetation, while two of them, Nos. 10 and 11, are situated near streams on the outermost part of the nearly flat area (at ∼85 m a.s.l.), characterized by wetland vegetation.

The majority of starting points have plan curvature characterized by small topographic depressions (see examples in Fig. 6; Nos. 5I, 5II, and 9). The rest are located on more uniformly sloping surfaces with no overall convex/concave trends (see example in Fig. 6; No. 12). The cross-profile of starting point No. 12 descends consistently westward with only minor surface variations. The starting points have no clear convex/concave trends in their profile curvature (see Fig. 6; No. 5I, 5II, 9 and 12).

In higher elevation areas of the mountain, the identification of starting zones on the images was more challenging due to the low-angle view of the photographs (see Fig. 3). As a result, 4 of the 12 mapped starting points are more uncertain than the rest (Nos. 1, 2, 7 and 8I, Fig. 5, Table 3) and their actual position may therefore be located at higher elevations than indicated on the maps. Not all flow paths captured in the photos were interpreted as slushflows. A relatively short flow path culminating in the nearly flat area, at ∼92 m a.s.l., was interpreted as an open stream due to the absence of snow transport along its course. Unlike slushflows, which always transport water-saturated snow, this open stream only flowed atop the snowpack. A few slushflows also appeared indistinct in the images due to image resolution limitations and were therefore not mapped. This indicates that the actual number of slushflows during this event may surpass the 12 that was mapped. The GIS-files of the mapped slushflow paths and starting points from all three events can be found in the supplementary material.

4.2. The 2023 event

For the 2023 event, six slushflows descending from elevations of up to ∼310 m a.s.l were identified on the imagery (Table 3; Fig. 5). The longest flow path (No. 8) covered a distance of >1000 m. Only five starting points were successfully identified, two of which converged into the same flow path (No. 6) downslope. Two starting points had plan curvature characterized by small topographic depressions, while the rest were located on more uniformly sloping terrain. Their profile curvature has no convex/concave trends. Three of the five identified starting points were more uncertain (Nos. 6II, 6III and 8I) than the rest. These three may be located at higher elevations than their mapped positions (Table 3). All slushflows, except No. 9, followed largely the same flow paths as the 2021 event, and three starting locations from both events (Nos. 6II, 10 and 11) were mapped in relatively close proximity to each other (<40 m apart). In the images, deposited snow occurred along some of the flow paths, particularly in the nearly flat area and further downslope towards the Rv-80. Fieldwork conducted on 27 January 2023, i.e. 2 days after the event, showed that slushflows had impacted the Rv-80 at three locations. The slushflow debris in these runout-zones contained only snow and very small amount of organic material, with no rock debris discovered during this fieldwork or subsequent fieldwork in June 2024.

4.3. The 2024 event

Analysis of the 2024 image dataset revealed the occurrence of seven slushflows (Table 3, Fig. 5). Due to flat light conditions and fog at the time of image acquisition, only fragments of the actual flow paths were visible for most of them. Only a single starting

https://doi.org/10.1017/jog.2025.10069 Published online by Cambridge University Press

Table 3. Mapped starting points, flow paths and length of flow paths, numbered from west to east

	Starting zones (and flow paths)	Longitude (UTM Zone 33)	Latitude (UTM Zone 33)	Elevation (m a.s.l.)	Flow path length (m)	Overlap (%) with modeled drainage routes	Overlap (%) with FKB-Vann
2021 Event	1	501268	7467812	265	199	9	0
	2 (a, b)	501324	7467817	263	632	8	7
	3	501412	7467760	206	267	35	0
	4 (a–c)	501843	7468103	300	1575	28	46
	5I	501914	7467961	253			
	5II	501953	7467924	241	782	46	76
	6I	502105	7468039	269			
	6II	502182	7468094	280	1602	42	56
	7	502318	7467812	162	889	42	43
	8I	502505	7467919	185			
	8II	502652	7468001	205	1113	54	70
	9	502762	7467998	201	473	65	64
	10	502556	7467588	85	257	33	4
	11	502613	7467607	89	370	54	–
	12	502938	7468062	236	388	28	60
2023 Event	6II	502148	7468070	277			
	6III	502232	7468003	253	700	16	28
	(7)			–	205	38	35
	8I	502455	7468201	312	1043	43	59
	(9)			–	442	39	19
	10	502572	7467595	87	271	35	7
	11	502661	7467603	85	170	44	
2024 Event	(2a)			–	61	5	0
	(4)			–	276	4	13
	(7)			–	389	23	33
	8I	502497	7467900	182	833	52	66
	(9)			–	110	20	62
	(10)			–	65	22	39
	(11)			–	112	67	–
					Mean:	34	36

Roman numerals indicate slushflows that initiate from separate starting locations and converge into the same flow path, while letters indicate slushflows that separate into multiple paths. The rightmost columns show overlap percentages between the mapped slushflows and modeled flow paths and FB-Vann. For slushflow path No. 11, no overlap was calculated due to the lack of FKB-Vann data in that area. All segments of each main slushflow path (e.g. No. 5) are joined in the statistical calculations.

point was identified (No. 8I), situated at ~180 m a.s.l. This starting point has no clear convex/concave trend in its plan or profile curvature. Further, No. 8I is located at nearly the same position as in the 2021 event (Table 3). The associated flow path covered a distance of ~750 m, following the same route as the two previous events. All of the seven flow paths mapped from the 2024 event followed largely the same routes as in 2021 and 2023 (Nos. 2, 4, 7, 8, 9, 10 and 11).

4.4. Comparison of mapped slushflows to modeled drainage pathways and the official surface water dataset of Norway ('FKB-Vann')

As noted in Section 3.3., FKB-Vann is produced by manual digitization on orthophotos. Some degree of variation in stream location between this dataset and the modeled drainage dataset is therefore expected. Since orthophotos used for digitization of FKB-Vann are recorded on clear summer days, water levels on the mountainside varies between years and almost certainly differ from winter conditions. Streams that are dry or periodically dry in summertime may therefore be absent in the FKB-Vann dataset.

Visual comparison indicates a general alignment between mapped slushflows and modeled flow paths (Fig. 7). Relatively good alignment is seen between slushflow paths Nos. 4, 5I, and 5II and the modeled drainage pathways. However, slushflows paths No. 2a-b, as well as smaller sections of paths Nos. 1, 6, 8 and 12, show little to no overlap. Among those that do overlap, their paths meander back and forth along the modeled drainage routes, rather than overlapping consistently along their entire course.

Statistical comparison of our mapped slushflows, with an assumed average width of 3 m, to the modeled drainage pathways yield an average overlap of 34% (Table 3). Statistical comparison of the mapped slushflows to FKB-Vann yields a similar average overlap of 36% (Table 3). Overlay analyses for statistical comparison were only performed when modeled pathways or FKB-Vann were in proximity to our mapped slushflows.

5. Discussion

5.1. Image analysis and comparison of the three events

Across all three events, a total of 25 slushflows were identified, only 5 of which had been previously registered in the national rapid mass movement database (see Section 2.2.). The starting zones were typically small and narrow, occurring at varying elevations on the mountainside in each event (Table 3). This is in accordance with Hestnes' (1998) and Thómasson and Hestnes' (2000) conclusion that slushflows may initiate at any elevation within a drainage basin when multiple slushflows are triggered in the same event. In areas with overlapping images from all three events (slushflows Nos. 4 and 6–11), all flow paths follow or closely align with established routes downslope, with only little variation between events. These routes mostly follow drainage pathways, some of which are relatively small and periodically dry.

Image analysis was influenced by the variation in spatial coverage between datasets. The 2021 dataset provided the most extensive overview of the mountainside, allowing many slushflows to be identified. In contrast, the images from the 2023 and 2024 events

https://doi.org/10.1017/jog.2025.10069 Published online by Cambridge University Press

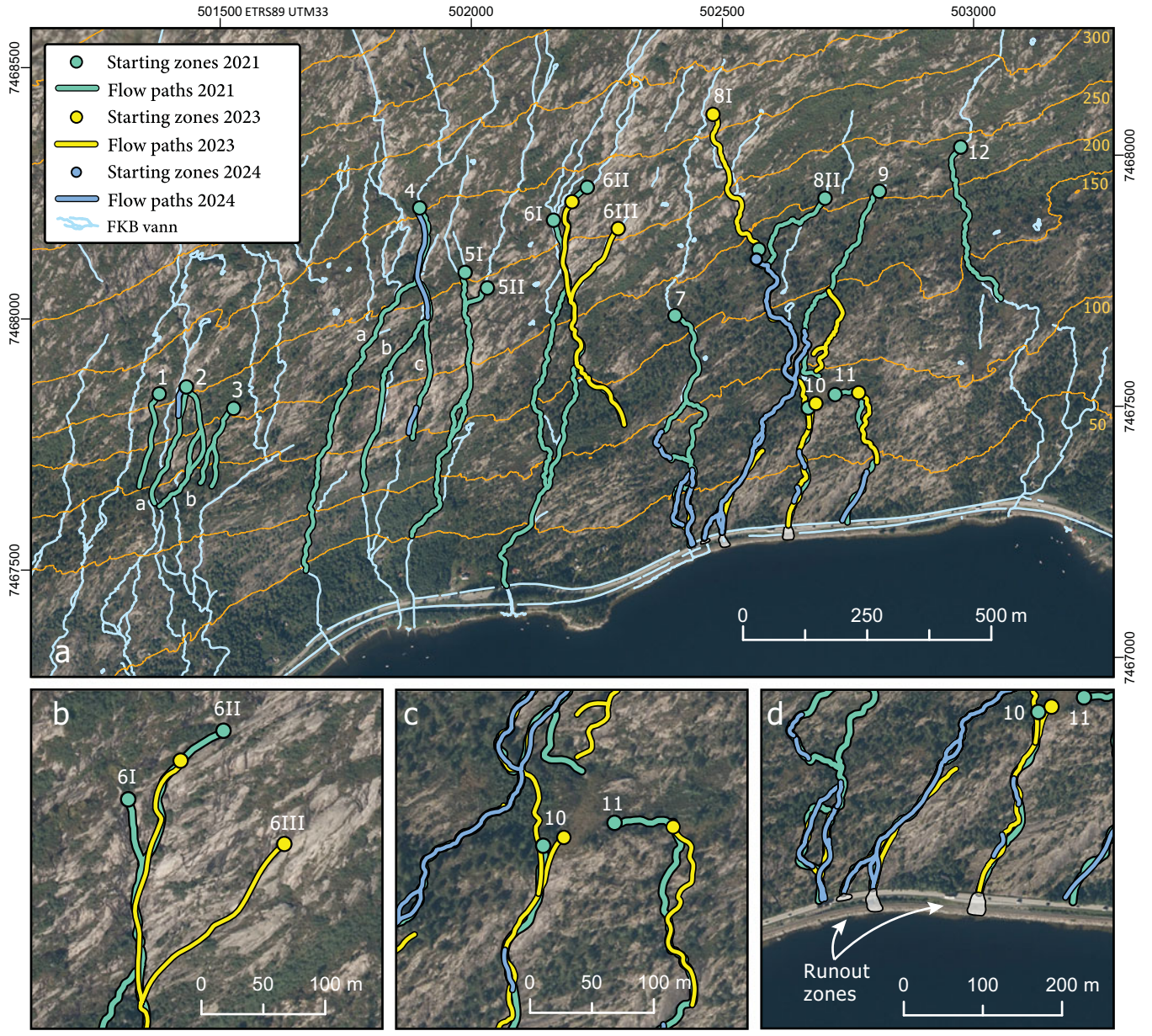

Figure 5. (a) Overview of starting points and flow paths at the field site for the three slushflow events, overlaid on FKB-Vann with contour lines at 50-m intervals. (b) Close-up of slushflows released in the 2021 and 2023 events on open, sparsely vegetated slopes. (c) Close-up of the nearly flat area where two slushflows (Nos. 10 and 11) were released during all three events. (d) Close-up of the area along the Rv-80 and railway impacted by snow deposition from flow paths Nos. 10 and 11 in all three events.

focused on the slushflows that deposited snow on the Rv-80 in the eastern part of the mountain and covered less than half the area captured in 2021 (Fig. 2). All three datasets included images recorded from a variety of angles. Oblique views were more helpful when mapping due to their broader spatial coverage and overview, compared to the detailed vertical images recorded from the same elevation. For all three events, image interpretation was considerably influenced by weather conditions at the time of image capture. Sparse rainfall followed by sub-zero temperatures prior to the 2021 event (Table 2) had led to ice patches forming on the westernmost mountain slopes, complicating slushflow identification. Ice patches were absent in the 2023 and 2024 imagery, but flat light conditions frequently obscured large sections of flow paths.

The differences in spatial coverage and visibility mean that direct comparisons between the different years are difficult. Although more slushflows were identified from the 2021 event than from the two later events, this is likely largely due to the greater spatial coverage. When looking at the areas which were mapped in all years, we find that in the 2023 event, starting point No. 8I (Fig. 5; Table 3) occurred at a higher elevation compared to the 2021 event. Additionally, slushflow path No. 6 displayed a different behavior as it initiated from a new starting position (Nos. 6II and 6III instead of 6I and 6II) and diverted from the 2021 course further downslope (Fig. 5). Slushflows were also more substantial in terms of width and volume of transported snow in the 2023 event, both along their trajectories and in the runout zone. For example, the nearly flat area was covered in slushflow deposits in 2023, but there was no sign of deposits in this area in the 2021 and 2024 imagery. This suggests that the scope of the 2023 event may have been at least equivalent to, if not surpassing the 2021 event, despite the lower

https://doi.org/10.1017/jog.2025.10069 Published online by Cambridge University Press

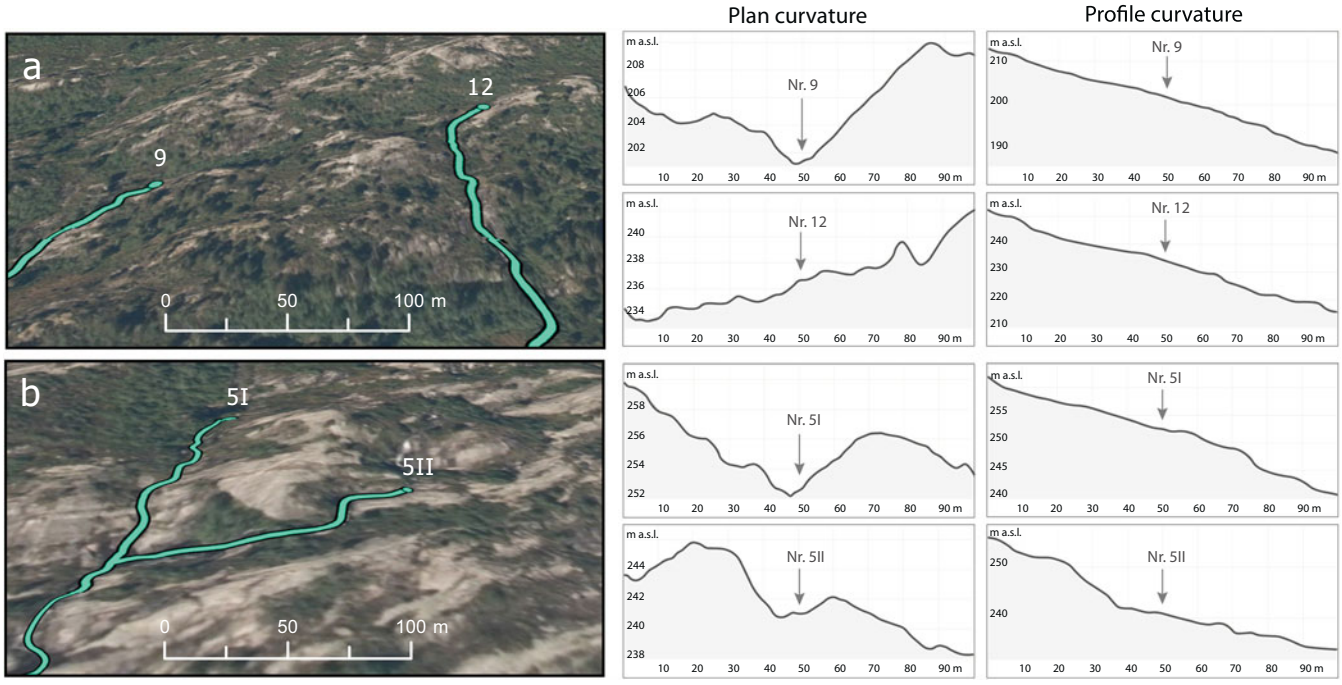

Figure 6. Plan and profile curvature for selected starting points 5I, 5II, 9 and 12 from the 2021 event. (a) The locations of Nos. 9 and 12 in the eastern part of the study area, where they initiated on slopes characterized by sparse tree cover. While No. 9 is located in a small topographic depression, No. 12 initiated on more uniformly sloping terrain with a cross-profile descending westward. (b) In the central part of the study area, starting points 5I and 5II are located in small topographic depressions where patches of shrub vegetation is interspersed among the exposed bedrock.

number of slushflows identified. For the 2024 event, only a single starting point and six fragmented flow paths were identified (Fig. 5; Table 3), something which, when considered alone, would point to a smaller slushflow event. However, the presence of fog in the 2024 images, especially at higher elevations, made starting points particularly difficult to identify. This may account for the fragmented flow paths and the low number of starting points identified for this event.

The starting points mapped at Kistrandfjellet vary slightly in terms of surrounding topography and substrate, with the majority situated close to or along streams on low-gradient open slopes marked by minimal or no vegetation, while Nos. 10 and 11 were positioned along streams in the nearly flat area (~85 m a.s.l.) covered with wetland vegetation. This is consistent with previous observations from Rana, northern Norway, where Hestnes and Sandersen (1987) found that sloping rock surfaces along drainage channels were the primary starting zones. Both plan and profile curvature at the locations of the mapped slushflow starting points were investigated (see Fig. 6 for examples). The plan curvature showed that approximately half of them were situated in small topographic depressions, demonstrating that slushflows not only initiate in shallow channels at the field site but also frequently initiate from locations where water flows over more uniformly sloping terrain. The profile curvature of nearly all starting points had no clear convex/concave trends.

5.2. Relationship between mapped slushflows, modeled drainage pathways and FKB-Vann

A comparison of the mapped slushflows to the modeled drainage pathways shows overlap along many flow paths (Fig. 7). However, the lack of overlap for flow paths No. 2a-b, and smaller sections of paths Nos. 1, 6, 8 and 12, indicates that these slushflows occurred in areas without permanent drainage. The image analysis identified two slushflows (Nos. 10 and 11, Fig. 5c) released at the outer edge of the nearly flat area, which is covered in wetland vegetation. These releases have generally taken place following those at higher elevations on the mountain (Andreassen, 2023). Such a delay in slushflow release, due to variations in small-scale topography and substrates, complicates the predictability and overall interpretation of slushflow activity on the mountain.

For the statistical analysis of overlap between the mapped slushflows and the modeled drainage and FKB-Vann datasets, the assumption of an average slushflow width of 3 m fit with our image interpretation. Increasing the slushflow width beyond the realistic size would have resulted in greater statistical overlap for some slushflows. However, the general picture would not have changed.

5.3. Slushflow management and documentation

Documenting and reporting individual flow paths and starting points is essential for several slushflow management tasks. High-quality spatial data on slushflows are, for example, essential for developing slushflow runout models. The data presented in this paper show a realistic scope of three slushflow events that took place at Kistrandfjellet, which in turn allows for a more precise evaluation of the issued early warning danger levels (Sund and others, 2024). During periods of active slushflow warnings, real-time reports of incidents, for example, via Varsom Regobs, may serve as valuable indicators of whether the assigned warning level is appropriate or requires adjustment. The reported incidents are transferred from Varsom Regobs to the national database and later also updated with additional information where available. Slushflow records are categorized according to four verifications

https://doi.org/10.1017/jog.2025.10069 Published online by Cambridge University Press

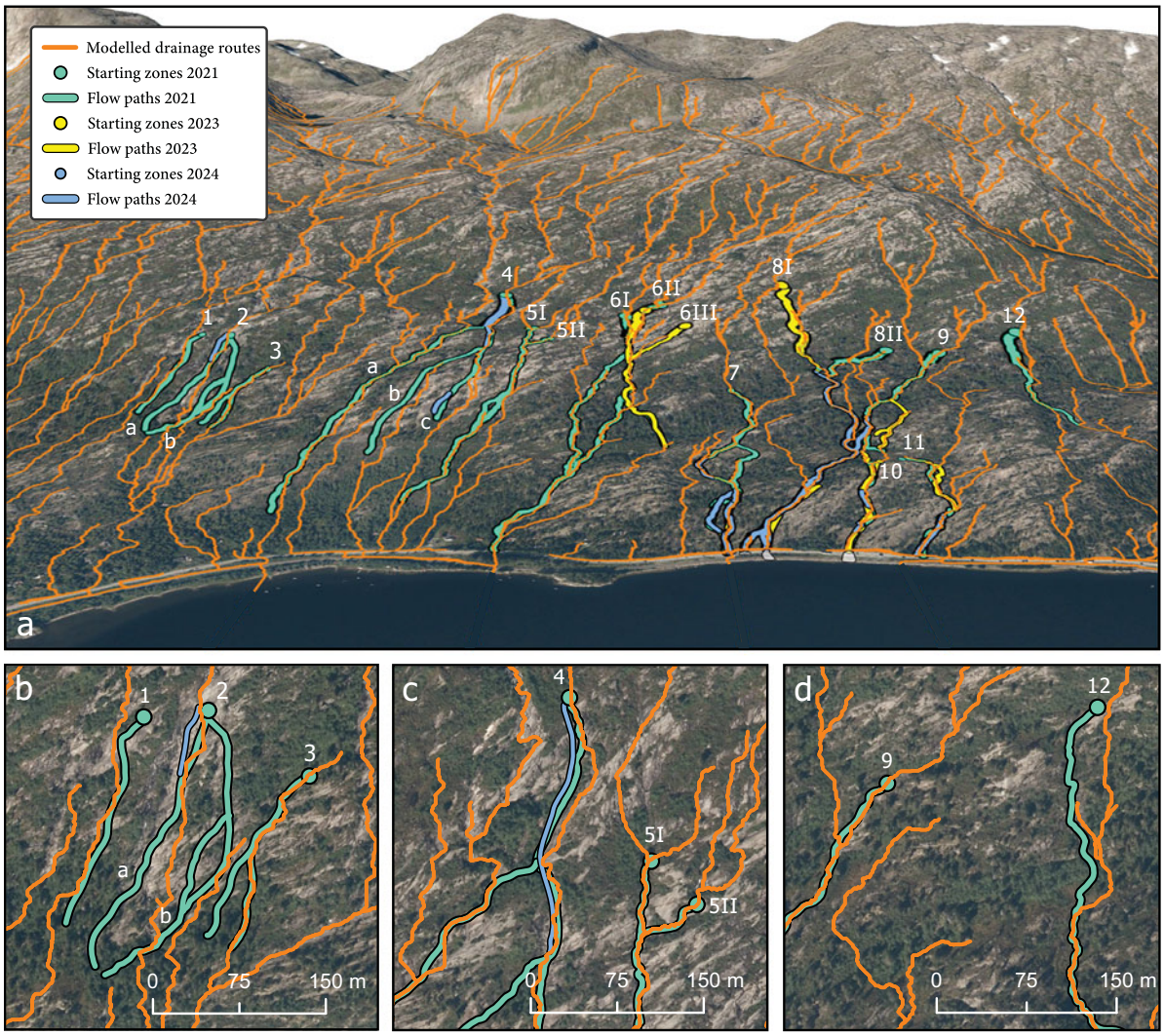

Figure 7. (a) Modeled drainage pathways (orange) on the mountain side using a DEM of 0.5 m resolution overlaid on mapped slushflows for the three events. (b) The westernmost part of the study area, showing weak overlap between the modeled drainage pathways and mapped slushflows. While flow paths Nos. 1 and 3 align with the modeled pathways in places, flow paths No. 2a-b show no alignment. (c) Relatively good alignment is seen between slushflow paths Nos. 4, 5I and 5II and the modeled drainage pathways. (d) In the easternmost part of the study area, slushflow path No. 12 displays minimal overlap with the modeled drainage pathways.

levels (A–D), ranging from well-documented incidents to those with uncertainties in location, mass movement type and timing (Lunde and others, 2023). An important aim is to increase the number of incidents in category A, where starting locations have uncertainty margins of $<\pm$100 m. Improved data on starting point locations can be used to acquire more accurate hydrological and meteorological data either from measurements or simulated grid values (Sund and others, 2024). For example, a difference of 100 m in elevation can constitute a large change in water supply values, even if the X, Y coordinates have an uncertainty of 100 m. This would be an important step toward developing a slushflow hazard early warning index, allowing for more automated steps in the hazard assessment that are currently performed manually.

Recent attempts have also been made to classify the most typical slushflow terrain types (Wasrud, 2021; Jaedicke and others, 2024). These studies show that improving the documentation of starting zones is necessary to achieve a better understanding of slushflow release. In turn, more precise data, such as those presented in this study, will also facilitate the development of susceptibility maps. This data is also necessary to develop numerical runout models tailored to slushflows, which would facilitate the identification of sites in need of mitigation measures. Such tools are not only relevant to researchers and slushflow professionals but also local municipalities and decision-makers involved in land-use planning. Several approaches have been tested (e.g. Bozhinskiy and Nazarov, 1998; Gauer, 2004; Jaedicke and others, 2008; Jónsson and Gauer, 2014). A study carried out by Skred (2021) hypothesized that the numerical runout model RAMMS::DEBRISFLOW may also be used for slushflow modeling. However, finding slushflow incidents with sufficient data quality proved challenging. Others have similarly pointed out that more data are needed to test the model for slushflow simulation (Hansen and others, 2024, 2024).

The quality of slushflow observations vary depending on the accessibility of the starting zone and the method and accuracy of data collection. In some cases, the starting zone of a slushflow can easily be documented and uploaded to Varsom Regobs. More often, however, starting zones are out of view from the observer, resulting in only the runout zone being documented. In these cases, use

https://doi.org/10.1017/jog.2025.10069 Published online by Cambridge University Press

of UAVs or other tools for gaining a high vantage point becomes necessary, such as the helicopter from which the 2021 event was documented. Based on our mapping, we recommend that future UAV-based documentation include capturing oblique views. While this approach is primarily relevant for those that have access to UAVs in their work, simpler yet valuable methods of data collection can also be effective for local observers or outdoor recreationists. For example, photographing the highest visible point of a flow path may facilitate subsequent work in locating the starting zone. When the distance is great, basic equipment such as binoculars may be used to capture closer views by photographing through the eyepiece.

To ensure that observations hold the highest quality possible, we suggest that consistent approaches and guidelines are established to standardize future data collection. Developing an official protocol for slushflow documentation will benefit the broader rapid mass movement research and management community. Input should be gathered from diverse stakeholders, including slushflow early warning personnel responsible for issuing bulletins and improving forecasting, road authorities and highway contractors handling road safety and slushflow incident reporting, as well as professionals engaged in research and hazard mitigation. Based on this input, standardized techniques can be established for conducting and recording field observations, with a particular focus on documenting starting zones, and for reporting through Varsom Regobs. These techniques should be tailored to two groups: professionals and recreationists, to facilitate data collection both along road networks and in remote areas.

6. Conclusion

Slushflow mitigation has suffered from a lack of documentation, which in turn has hampered the management of this natural hazard. Identifying starting points, along with enhancing the quality of slushflow documentation, would greatly benefit the management of slushflows.

In this study, we have quantified the difference between registered and actual slushflows. We used unique image datasets for Kistrandfjellet, northern Norway, covering three major slushflow events in February 2021, January 2023 and January 2024. Mapping revealed the occurrence of at least 25 slushflows across all three events: 2021 (12), 2023 (6) and 2024 (7). For the 2021 event, this amounted to six times the official number recorded in the rapid mass movement database. For the 2023 and 2024 events, the official number of registered slushflows was two and one, respectively. The 2021 dataset provided the greatest spatial coverage of the field site.

Starting points were identified at different elevations on the mountain slopes: ~85–300 m a.s.l. (2021), ~85–312 (2023) and ~182 m a.s.l. (2024). Investigation of plan curvature at the starting point locations showed that while many slushflows initiated in small topographic depressions, others initiated on more uniformly sloping terrain. The profile curvature of the starting locations generally showed no convex/concave trend. The longest flow paths covered distances of ~900 m, >1000 m and ~750 m in the 2021, 2023 and 2024 events, respectively.

Drainage pathways were modeled using a high-resolution DEM of 0.5 m. Statistical comparison of mapped slushflows with modeled drainage pathways yielded an average overlap of 34%. Similarly, comparison of the mapped slushflows to the FKB-Vann dataset yielded an average overlap of 36%.

For effective slushflow management, high-quality documentation and data on starting locations are important to advance the regional early warning of slushflows, develop slushflow-tailored numerical runout models, and produce susceptibility maps. To improve slushflow documentation, consistent approaches and guidelines must be established to standardize future data collection.

Supplementary material. The supplementary material for this article can be found at 10.1017/jog.2025.10069.

Acknowledgements. We thank the 330 squadron, Royal Norwegian Air Force, and the Norwegian Public Roads Administration for providing the slushflow image datasets used in this study. We are grateful to the Hans og Helga Reuschs Legacy and the Statsminister Gunnar Knudsen og hustru Sofie født Cappelens Family Legacy for funding fieldwork equipment. We also thank two anonymous reviewers for valuable comments that helped to improve this paper.

Competing interests. The authors declare none.

References

Andreassen DT (2023) *Slush Flows on Highway RV80 to the City of Bodoe, Northern Norway*. *Proceedings* Bend, Oregon: *International Snow Science Workshop*, 726–728.

Andreassen DT, Kvalvågnes J, Bohlin I and Rasmussen E (2024) Site-specific slush flow warning on highway RV80, northern Norway. *Proceedings of the International Snow Science Workshop, Tromsø, Norway*, 750–753.

Avisa Nordland (2024) Riksvei 80-stenging koster enorme summer: Kommuner har satt inn ekstra beredskap, 12 January 2024. Available at https://www.nb.no/items/e663411260f476532415f0f7d324511d?page=7&searchText=%225,6%20millioner%22%20Riksvei%2080 (Last accessed 15 November 2024)

Bozhinskiy AN and Nazarov AN (1998) Dynamics of two-layer slushflows. In Hestnes E (ed), *25 Years of Snow Avalanche Research*. Oslo, Norway: NGI Publication 203, 74–78. Proceedings of a Conference at Voss, Norway

Clark MJ and Seppala M (1988) Slushflows in a subarctic environment, Kilpisjarvi, Finnish Lapland. *Arctic and Alpine Research* **20**(1), 97–105. doi:10.1080/00040851.1988.12002655

Decaulne A and Sæmundsson Þ (2006) Meteorological conditions during slush-flow release and their geomorphological impact in northwestern Iceland: A case study from the Bíldudalur valley. *Geografiska Annaler, Series A, Physical Geography* **88**(3), 187–197. doi:10.1111/j.1468-0459.2006.00294.x

Eiken T and Sund M (2012) Photogrammetric methods applied to Svalbard glaciers: Accuracies and challenges. *Polar Research* **31**. doi:10.3402/polar.v31i0.18671

Ekker R, Kværne K, Os A, Humstad T, Wartiainen A, Eide V and Hansen RK (2013) regObs – Public database for submitting and sharing observations. In *Proceedings of the International Snow Science Workshop*. Grenoble, France: 461–465.

Gauer P (2004) Numerical modeling of a slush flow event. In *Proceedings of the International Snow Science Workshop*. Wyoming: Jackson Hole, 39–43.

Geonorge (2024) FKB vann. Available at: https://register.geonorge.no/register/versjoner/produktspesifikasjoner/geovekst/fkb-vann (Last accessed 20 May 2024)

Hansen VE (2024) *Investigating limitations of RAMMS:Debrisflow as a slushflow simulation tool: Using numerical modelling as a tool to predict slushflow runouts*. M.Sc. thesis, Department of Geoscience, The Arctic University of Norway (UiT), Tromsø, Norway.

Hansen VE, D'Amboise CJL and Vick LM (2024) Limitations of RAMMS:DEBRISFLOW as a slushflow simulation tool. In *Proceedings of the International Snow Science Workshop*. Tromsø, Norway: 792–798.

Hestnes E (1985) A contribution to the prediction of slush avalanches. *Annals of Glaciology* **6**, 1–4. doi:10.3189/1985AoG6-1-1-4

Hestnes E (1998) Slushflow hazard - where, why and when? 25 years of experience with slushflow consulting and research. *Annals of Glaciology* **26**, 370–376. doi:10.3189/1998AoG26-1-370-376

Hestnes E, and **Kristensen** (2010) The diversities of large slushflows illustrated by selected cases. In *Proceedings of the International Snow Science Workshop*. California: USA, 348–355.

Hestnes E and Bakkehøi S (2004) Slushflow hazard prediction and warning. *Annals of Glaciology* **38**, 45–51. doi:10.3189/172756404781814889

Hestnes E, Bakkehøi S and Kristensen K (2012) Slushflow formation, flow regimes and consequences. In *Proceedings of the International Snow Science Workshop*. Anchorage, Alaska: 414–419.

Hestnes E, Bakkehøi S, Sandersen F and Andresen L (1994) Weather and snowpack conditions essential to slushflow release and downslope propagation. In *Proceedings of the International Snow Science Workshop* 1994. Snowbird, Utah, USA: 40–57.

Hestnes E and Jaedicke C (2018) Global warming reduces the consequences of snow-related hazards. In *Proceedings of the International Snow Science Workshop*. Innsbruck, Austria: 493–497.

Hestnes E and Sandersen F (1987) Slushflow activity in the Rana district, North Norway. *In*: *Proceedings of the Davos Symposium*. IAHS Publication, 317–330.

Hestnes E and Sandersen F (2000) The main principles of slushflow hazard mitigation. *In*: *Internationales Symposion Interpraevent 2000*. Villach, Austria, Tagungspublikation, Band: 2, 267–280.

Hoydedata (2017) 0.5m and 1m DEMs. NDH Bodø 2kt 2017 (0.5 m, 4-09-2022) : https://hoydedata.no/LaserInnsyn2/ (Last accessed 24 March 2025).

Jaedicke C, Kern MA, Gauer P, Baillifard MA and Platzer K (2008) Chute experiments on slushflow dynamics. *Cold Regions Science and Technology* **51**(2-3), 156–167. doi:10.1016/j.coldregions.2007.03.011

Jaedicke C, Sund M, Grímsdóttir H, Helgason JK, Bartsch UBA, Sandersen F and Morken E (2024) Classification of slushflow release areas in Norway and Iceland. *Proceedings of the International Snow Science Workshop, Tromsø, Norway* 785–791.

Jónsson Á, and Gauer P(2014) Optimizing mitigation measures against slush flows by means of numerical modelling - A Case Study Longyearbyen, Svalbard. In *Extended Abstracts of the INTERPRAEVENT 2014*. Nara, Japan: The research society INTERPRAEVENT: 727–732.

Luckman B (1977) The geomorphic activity of snow avalanches. *Geografiska Annaler. Series A, Physical Geography* **59**(1), 31–48. doi:10.2307/520580

Lunde EN, Morken E, Devoli G and Sund M (2023) Registrerte og kontrollerte sørpeskred i Norge, Statistisk oversikt og metodegrunnlag. NVE report 8-2023, 1-26, https://publikasjoner.nve.no/rapport/2023/rapport2023_31.pdf (Last accessed 03 February 2024)

Norgeibilder (2022) Ortophotos. Bodø 2022 (0.08 m, 10-06-2022) : https://www.norgeibilder.no/ (Last accessed 17 July 2025).

Norwegian Centre for Climate Services (2022) Klimaprofil Nordland. Available at: https://klimaservicesenter.no/kss/klimaprofiler/nordland (Last accessed 15 November 2024)

Norwegian Centre for Climate Services (2025) Observations and weather statistics. Available at: https://seklima.met.no/observations/ (Last accessed 20 January 2025)

NVE (2021) Varsom Regobs. https://www.regobs.no/registration/257613 (Last accessed 09 May 2025)

NVE (2023) Varsom Regobs. https://www.regobs.no/registration/322704 (Last accessed 09 May 2025)

NVE (2024) Varsom Regobs. https://www.regobs.no/registration/362433 (Last accessed 09 May 2025)

Nyberg R (1985) Debris flows and slush avalanches in northern Swedish Lappland. Distribution and geomorphological significance. *Meddelanden Från Lunds Universitets Geografiska Institution – Avhandlingar* **97**, 1.

Nyberg R (1989) Observations of slushflows and their geomorphological effects in the Swedish mountain area. *Geografiska Annaler, Series A, Physical Geography* **71**(3), 185–198.

Onesti LJ (1985) Meteorological conditions that initiate slushflows in the Central Brooks Range, Alaska. *Annals of Glaciology* **6**, 23–25. doi:10.3189/1985AoG6-1-23-25

Onesti LJ and Hestnes E (1989) Slush-flow questionnaire. *Annals of Glaciology* **13**, 226–230. doi:10.3189/S0260305500007941

Perov VF (1998) Slushflows: Basic properties and spreading. *NGI Publication* **203**, 203–209.

Rapp A (1960) Recent development of mountain slopes in Kärkevagge and surroundings, northern Scandinavia. *Geografiska Annaler* **42**(2/3), 65–200. doi:10.1080/20014422.1960.11880942

SeNorge (2025) Snow depth data. Available at: https://www.senorge.no/ (Last accessed 15 June 2025)

Skred AS (2021) Bruk av RAMMS::DEBRISFLOW på kjente sørpeskredhendelser NVE external report 9-2021. Available at: https://publikasjoner.nve.no/eksternrapport/2021/eksternrapport2021_09.pdf (Last accessed 02 February 2025)

Sund M, Grønsten HA and Seljesæter SÅ (2024) A regional early warning for slushflow hazard. *Natural Hazards and Earth System Sciences* **24**, 1185–1201. doi:10.5194/nhess-24-1185-2024

Svendsen SP, Gjermundsen EF, Sund M and Anjar J (2024) Slushflow documentation: Possibilites and limitations. In *Proceedings of the International Snow Science Workshop*, Tromsø, Norway: 773–777.

Thómasson GG and Hestnes E (2000) Slushflow Hazard and Mitigation in Vesturbyggd, Northwest Iceland. *Nordic Hydrology* **31**(4/5), 399–410. doi:10.2166/nh.2000.0024

Washburn AL and Goldthwait RP (1958) Slushflows. *Geological Society of America* **69**, 1657–1658.

Wasrud J (2021) Identifisering av løsneområder for sørpeskred: Klassifikasjon og beskrivelse av de mest løsneområdene for sørpeskred. NVE report 08-2021, 1-29, https://publikasjoner.nve.no/eksternrapport/2021/eksternrapport2021_08.pdf (Last accessed 03 February 2025)

https://doi.org/10.1017/jog.2025.10069 Published online by Cambridge University Press